Stereoscopic PIV using optical flow: investigation of a recirculating cavity flow

Thierry M. Faure, Christelle L. Douay, Sépass Mochki, François Lusseyran, Georges Quénot

STEREOSCOPIC PIV USING OPTICAL FLOW: INVESTIGATION OF A RECIRCULATING CAVITY FLOW

T.M. Faure[1], C.L. Douay[1], S. Mochki[1], F. Lusseyran[1], and G.M. Quénot[2]

[1]LIMSI-CNRS, UPR 3251, Université Pierre et Marie Curie, Paris 6 et Université Paris-Sud 11, Bât. 508, rue J. Von Neumann, B.P. 133, 91403 Orsay Cedex
[2]CLIPS-CNRS, UMR 5524, 385 rue de la Bibliothèque, B.P. 53, 38041 Grenoble Cedex 9

thierry.faure@limsi.fr

Abstract

Experimental measurement of the three components of velocity inside a plane is addressed with the stereoscopic particle image velocimetry (PIV) using an optical flow algorithm. This technique is a valuable diagnostic tool for quantitative instantaneous description of three-dimensional (3D) turbulent flows, as those dominated by vortex motion.

1 Introduction

PIV is a measurement technique which is valuable for quantitative description of flows (Raffel et al., 1998). Thanks to the development of high-speed cameras and high repetition rate lasers, it is now possible to explore turbulent flows. The observation

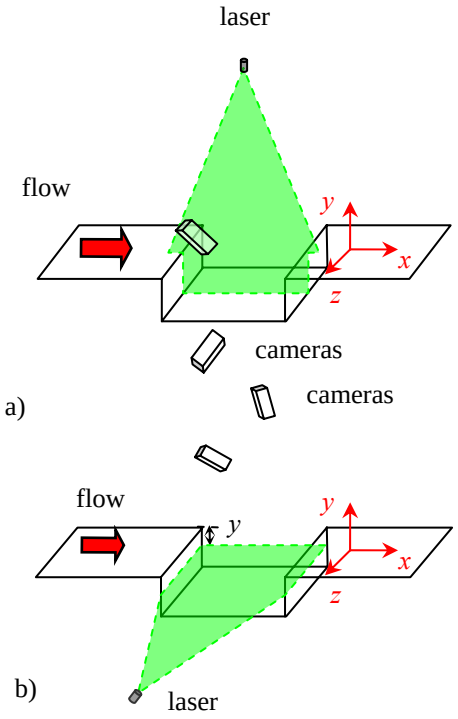

Figure 1: Measurement planes: a) (x,y) plane or b) (x,z) plane inside the cavity.

with two cameras provides the field of three components of velocity (3C) inside a laser plane (2D). The stereoscopic PIV algorithm implemented for this study is an optical flow using dynamical programming. After a description of the experimental set-up and apparatus, the PIV system calibration procedure is exposed, permitting the localization of the two cameras relatively with the laser plane. The present study focuses on a recirculation cavity flow, where instabilities associated with vortices are present. Measurements in two different planes are explored permitting comparison between 2C-2D PIV and 3C-2D PIV. The main flow features and development of a Taylor-Görtler-like instability are also discussed.

2 Experimental set-up

The cavity length L and depth H define aspect ratio L/H which is varied between 0.5 and 2, its span $S = 0.3$ m is constant, x is the external flow direction, y the cavity depth axis and z is the cavity span direction. The flow is considered for Reynolds numbers, based on the external velocity U_e and the cavity depth, ranging from 860 to 37 000. Hereafter, the expressions “upstream” and “downstream” will refer to the external velocity direction. The origin of the Cartesian coordinate system is placed at the upstream edge of the cavity at mid-span. PIV measurements are conducted with a pulsed YAG laser emitting a 0.25 mm thick light sheet at 532 nm during 6 ns with energy of 200 mJ per pulse. The image recording system consists of a 10-bit camera with 1 032×778 pixels and a frequency of 20 Hz. The camera focal length is 25 mm. Two observation planes are considered. A (x,y) plane is explored with one camera in the cavity span axis, allowing a comparison with the 2C-2D PIV optical flow algorithm (Figure 1-a). A (x,z) plane situated at $y/H = -0.3$ is also studied for a complete description of the three-dimensional flow motion (Figure 1-b). It has been shown that the cavity recirculation is dominated by a primary vortex of spanwise axis (Faure et al., 2007). For particular parameters, a centrifugal Taylor-Görtler-like instability is also present as pairs of quasi-annular counter-rotating vortices superimposed with the primary vortex (Faure et al., 2009-a).

3 PIV algorithm

In this work, PIV images are analyzed with an optical flow algorithm using orthogonal dynamic programming (Quénot et al., 1998). This advanced PIV method is based on an iterative search of a global alignment of particle images, with regularity and continuity constraints (minimization of a Minkowski norm). The particle image displacement problem inside a plane is reduced to a one-dimension problem, considering the displacement in one direction within a given analysis strip. The two-dimensional solution is obtained by successive iterative resolution within smaller and smaller orthogonal strips. The main advantages of this stable and accurate method are:

- it can be used for sequences of two images or more;
- it provides highly resolved displacement fields with one vector per pixel;
- the velocity field is continuous and differentiable, which is particularly adapted for strong velocity gradient flows;
- it can be generalized to stereoscopic PIV to provide three velocity components, this version of the algorithm being the object of this study.

Its principal drawbacks are:

- large computation time without exceeding advanced algorithms using cross-correlation and image deformation (Scarano, 2001);
- adjustment of many parameters and their sensitivity to flow configuration.

The optical flow resolution is 1 / 32nd pixel or, in the present case, a relative velocity accuracy of 0.15%. The stereoscopic version of the optical flow PIV algorithm is implemented in this work

4 Stereoscopic PIV calibration

The calibration of the two cameras is included in the procedure based on a pinhole model (Quénot, 2001). Each camera calibration is computed from a single view of a target placed in the laser plane and the camera focal length. The target is a planar image of black disks, placed on a squared grid, on a white background (Figure 2 a-b). In order to unambiguously determine the target origin and orientation, the disks whose coordinates, in grid step units, are (0,0), (3,0) and (0,2) are removed. A camera calibration program generates, from the image of the target, the camera position from the center of the target (distances and angles). The image rectification is then possible, providing, from the recorded images of the target by each camera, a recreated view in the target coordinate system (Figure 2 c-d).

For present measurements, the image sharpness criterion is not strictly checked because we do not use Scheimpflug mounts between each camera sensor and lens. However, sharp enough image recording is possible because of the choice of a small angle between the two cameras $\theta \approx 20$ deg. This limited angle is of course altering the resolution on the velocity component orthogonal to the measurement plane.

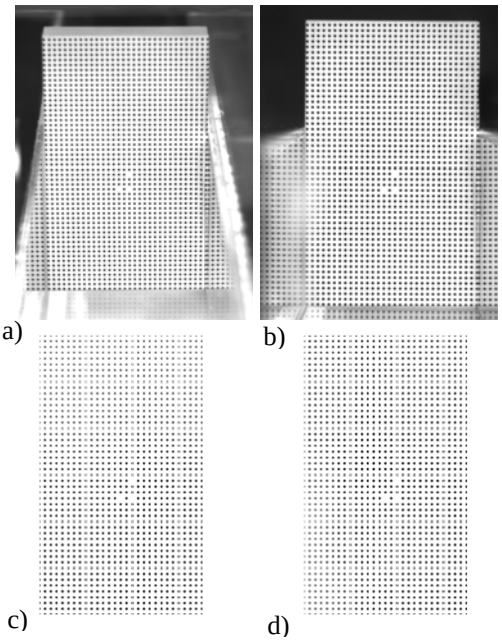

Figure 2: Calibration target observed by a) camera 2, b) camera 1 and c), d) rectification of the images of the target.

5 Velocity reconstruction

The camera magnification is (Figure 3):

$$M = \frac{X_2 - X_1}{x_1 - x'_2} \qquad (1)$$

where x_1 and x_2 are the true particle displacement in the laser sheet, x'_2 is the projection of this displacement in the (x,y) plane and X_1 and X_2 the observed displacement in the image plane (camera sensor).

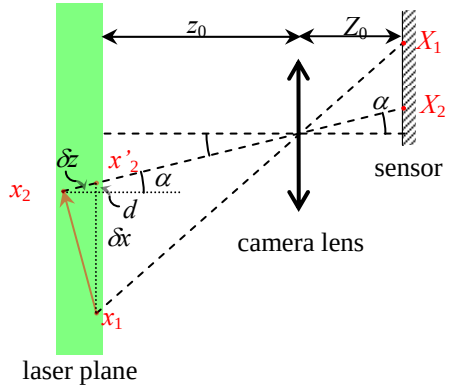

Figure 3: Displacement inside the laser sheet measured by the camera.

Inside the (x,z) plane, the observed displacement is:

$$x'_2 - x_1 = \delta x + d \qquad (2)$$

Thus, the angle α inside the (x,z) plane is defined by:

$$\tan\alpha = \frac{d}{\delta z} = \frac{X_2}{Z_0} \tag{3}$$

The displacement inside the image plane is:

$$X_2 - X_1 = -M\left(\delta x + \delta z \frac{X_2}{Z_0}\right) \tag{4}$$

We get the same expression in the (y,z) plane with an angle β:

$$Y_2 - Y_1 = -M\left(\delta y + \delta z \frac{Y_2}{Z_0}\right) \tag{5}$$

For a stereoscopic system of two cameras, the velocity components measured are respectively, for the first camera:

$$U_1 = \frac{\delta x + \delta z \tan\alpha_1}{\delta t} \quad V_1 = \frac{\delta y + \delta z \tan\beta_1}{\delta t} \tag{6}$$

A similar expression is found for the second camera with angles α and β, providing the expressions of the velocity components:

$$U_x = \frac{U_1 \tan\alpha_2 - U_2 \tan\alpha_1}{\tan\alpha_2 - \tan\alpha_1} \tag{7}$$

$$U_y = \frac{V_1 \tan\beta_2 - V_2 \tan\beta_1}{\tan\beta_2 - \tan\beta_1} \tag{8}$$

$$U_z = \frac{U_1 - U_2}{\tan\alpha_1 - \tan\alpha_2} = \frac{V_1 - V_2}{\tan\beta_1 - \tan\beta_2} \tag{9}$$

If the cameras are positioned alongside y-axis, then angles α_1 and α_2 are small and a better estimate of the velocity components is given by:

$$U_x = \frac{U_1 + U_2}{2} - \frac{V_1 - V_2}{2} \frac{\tan\alpha_1 + \tan\alpha_2}{\tan\beta_1 - \tan\beta_2} \tag{10}$$

$$U_y = \frac{V_1 \tan\beta_2 - V_2 \tan\beta_1}{\tan\beta_2 - \tan\beta_1} \tag{11}$$

$$U_z = \frac{V_1 - V_2}{\tan\beta_1 - \tan\beta_2} \tag{12}$$

Then, if the measurement error is ε_1 for the first camera and ε_2 for the second camera and with angles $\beta_1 \approx 0$ deg and $\beta_2 \approx 20$ deg:

$$\varepsilon_{U,x} \approx \frac{\varepsilon_1 + \varepsilon_2}{2} \tag{13}$$

$$\varepsilon_{U,y} \approx \varepsilon_1 \tag{14}$$

$$\varepsilon_{U,z} \approx \frac{\varepsilon_1 + \varepsilon_2}{\tan\beta_2} \tag{15}$$

Assuming $\varepsilon_1 = \varepsilon_2 = \varepsilon$ we get:

$$\varepsilon_{U,x} \approx \varepsilon\,;\, \varepsilon_{U,y} \approx \varepsilon\,;\, \varepsilon_{U,z} \approx 6\varepsilon \tag{16}$$

With that setting, the relative accuracy on the velocity component orthogonal to the measurement plane is found to 0.9%.

6 Results

For measurements in the (x,y) plane, and L/H = 1, the first camera is perpendicular to the laser plane (Figure 4) and the angle between cameras is $\theta \approx 20$ deg. The instantaneous flow streamlines clearly identifies the vortex of spanwise axis inscribed inside the cavity (Figure 5). Furthermore, as one camera is aligned with the cavity axis, a comparison between stereoscopic 3C-2D PIV and classical 2C-2D PIV is given. The velocity profiles along the y-direction passing through the center of the spanwise vortex show a good agreement between the two algorithms (Figure 6). The axial velocity component presents a large gradient in the shear-layer region developing between the cavity and the external flow. A small region of negative velocity is observed at the bottom of the cavity, corresponding to the clockwise flow rotation. The y-velocity component is much smaller and close to zero at the cavity top and bottom where the flow direction is horizontal.

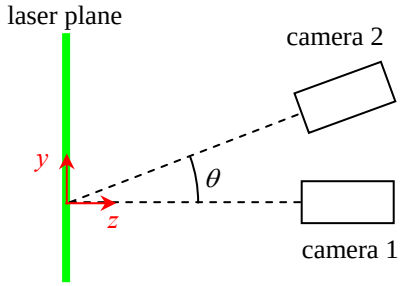

Figure 4: Positions of the cameras for 2C-PIV and 3C-PIV comparison.

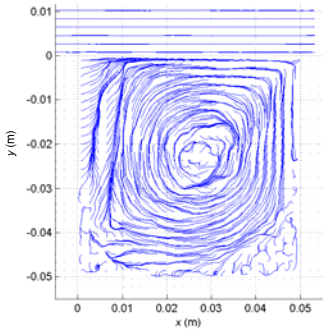

Figure 5: Streamlines for Re_H = 4,230 and L/H = 1.

Measurements are also made in a (x,z) plane to understand the development of a raw of Taylor-Görtler-like counter-rotating vortices previously observed (Figure 7).The instantaneous flow streamlines in the (x,z) plane are superimposed with the y-velocity component (Figure 8). The two lateral white stripes are shadow zones which are not viewed by the two cameras. The flow near the upstream edge of the cavity presents positive values of U_y while the downstream edge of the cavity shows negative values of U_y, both corresponding to the recirculation motion of the vortex of spanwise axis. In addition, the spanwise modulation of regions of maximum or minimum values of U_y is correlated with the position of the quasi-annular Taylor-Görtler-like centrifugal vortices.

As the cavity flow is three-dimensional, and dominated by the primary vortex motion, the measurement PIV fields in the (x,z) plane are carried out with a large velocity component perpendicular to the measurement plane, whose velocity is 5 times larger than the velocity of Taylor-Görtler-like centrifugal vortices. Then, a two-component measurement is subject to projection effect away from the optical axis.

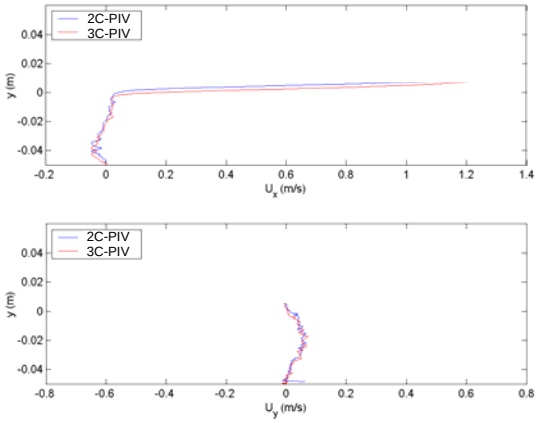

Figure 6: Velocity profiles along the diameter of the recirculation vortex (x/L = 0.5): comparison between 2C-PIV and 3C-PIV.

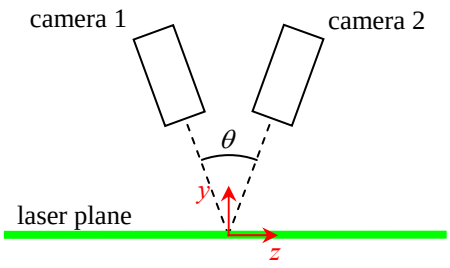

Figure 7: Positions of the cameras for 3C-PIV measurements inside a (x,z) plane.

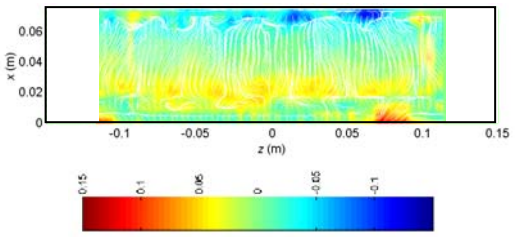

Figure 8: Streamlines of (U_x, U_z) inside the (x,z) plane and U_y velocity component measured by stereoscopic PIV for L/H = 1,5, Re_H = 4 450 inside a plane y/H = – 0,3.

7 Vortex identification

These stereoscopic measurements also validate previous analyses conducted with two-component PIV, about the size and wavelength of centrifugal vortices identified for some parameters (Faure et al., 2008). Above a threshold, a raw of pairs of counter-rotating vortices appears inside the cavity. These vortices are generated by the flow curvature induced by the primary vortex of spanwise axis, and present a quasi-annular pattern. In order to locate the vortices, the Γ_2 criterion is applied (Michard and Favelier, 2004). It is an Eulerian criterion which is a normalized kinetic moment considering the relative motion around a given position, defined as:

$$\Gamma_2(\vec{x}) = \frac{1}{S}\int_{\vec{x}'\in S} \frac{(\vec{x}'-\vec{x})\wedge\left[\vec{U}(\vec{x}')-\vec{U}(\vec{x})\right]}{\left\|\vec{x}'-\vec{x}\right\|\left\|\vec{U}(\vec{x}')-\vec{U}(\vec{x})\right\|}d\vec{x}' \qquad (17)$$

In equation (17), S is a domain containing the position $\vec{x}$. The main advantage of this criterion over other identification tools is that it is Galilean invariant. It is applied on an instantaneous field and underlines the location of the pairs of counter-rotating vortices associated with zones where the Γ_2 criterion is close to –1 or 1 (Figure 9). In particular, the raw present near the upstream cavity edge is found as observed in flow visualizations (Faure et al., 2009-a) and 2C-2D PIV measurements (Faure et al., 2009-b).

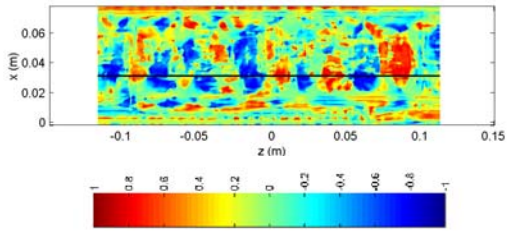

Figure 9: Γ_2 criterion measured by stereoscopic PIV for L/H = 1,5, Re_H = 4 450 inside a plane y/H = – 0,3.

It has been shown (Faure et al. 2007) that the spanwise raw of vortices resulting of the centrifugal instability are migrating from the cavity centerline outward the cavity sides. This drift motion is due to the spanwise flow in the inner part of the cavity from the sides toward the centerline. The spanwise drift velocity W_s is measured from space-time diagrams. They are built stacking, over each other, a horizontal line of the Γ_2 field chosen in a region where a row of vortices is present (black line in Figure 9), at different successive times. On such diagrams, vertical lines are associated to stationary events, while oblique lines are associated to traveling patterns (Figure 10). If oblique lines are moreover straight lines, it means that the pattern is traveling at a constant velocity. As these lines have a slope between zero and a maximum value, we choose to characterize each configuration with a maximum spanwise drifting velocity W_s. The measurement of W_s/U_e brings to 0.0068 which is in good agreement with the value 0.0064 obtained with 2C-2D PIV and flow visualizations.

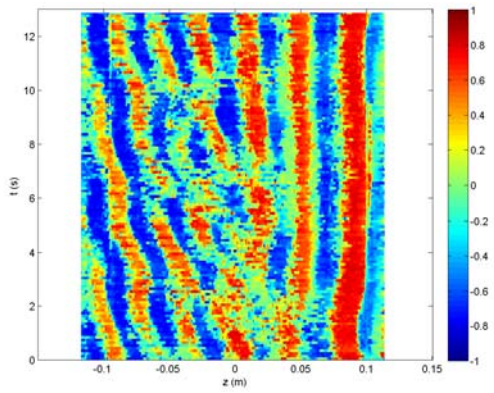

Figure 10: Space-time diagram of the Γ_2 criterion for L/H = 1,5, Re_H = 4 450.

8 Conclusions

The three components of the velocity have been investigated with a stereoscopic PIV technique in a cavity recirculation flow, showing development of a Taylor-Görtler-like instability. Although Scheimpflug mounts are not used, stereoscopic measurements provide three components of velocity field with an estimated error six times greater for the component perpendicular to the measurement plane, but still reasonable since it is found to be 0.9%. The first perspective of that study is the implementation of Scheimpflug mounts on cameras to increase their angle and evaluate the incidence on image sharpness. The second objective is the simultaneous stereoscopic PIV measurements in two orthogonal planes, in order to understand the coupling between the recirculating flow in the (*x*,*y*) plane, and the development of the Taylor-Görtler-like instability in the (*x*,*z*) plane.

References

Faure, T.M., Adrianos, P., Lusseyran, F., Pastur, L.R. (2007) Visualizations of the flow inside an open cavity at medium range Reynolds numbers, *Exp. Fluids*, Vol. 42, No. 2, pp. 169–184

Faure, T.M., Defrasne, A., Lusseyran, F., Pastur, L.R. (2008) Flow instabilities development inside an open cavity, *13th International Symposium on Flow Visualization*, Nice (France), July 1-4 2008, Paper ID 81

Faure, T.M., Pastur, L.R., Lusseyran, F., Fraigneau, Y., Bisch, D (2009-a) Three-dimensional centrifugal instabilities development inside a parallelepipedic open cavity of various shape, *Exp. Fluids*, Vol. 47, No. 3, pp. 395–410

Faure, T.M., Lefèvre, G., Pastur, L.R., Lusseyran, F. (2009-b) Critères d'apparition d'instabilités centrifuges dans une cavité ouverte, *19ème Congrès Français de Mécanique*, Marseille (France), 24-28 août 2009

Michard, M., Favelier, T. (2004) Développement d'un critère d'identification de structures tourbillonnaires adapté aux mesures de vitesse par PIV, *9ème Congrès Francophone de Vélocimétrie Laser*, Bruxelles (Belgique), 14-17 septembre 2004

Quénot, G.M., Pakleza, J., Kowalewski, T.A. (1998) Particle image velocimetry with optical flow, *Exp. Fluids*, Vol. 25, No. 3, pp. 177–189

Quénot, G.M. (2001) Camera calibration using a single target image and camera focal length, *Fourth International Workshop on Particle Image Velocimetry*, paper 1040, Göttingen, Germany, 17-19 September 2001

Scarano, F. (2001) Iterative image deformation method in PIV – Review article – *Meas. Sci. Techno.*, Vol. 12, pp. 1382–1391

Raffel, M., Willert, C.E., Kompenhans, J. (1998) *Particle Image Velocimetry, A Practical Guide*, Springer